

Improved performance of nanocomposite forward osmosis membrane with polydopamine nanoparticles/polyphenylsulfone (PDA Nps/PPSU) substrate and UV irradiation treated polycarbonate active layer

Ali Borsalani, Seyed Mostafa Tabatabaee Ghomsheh*, Alireza Azimi, Masoomeh Mirzaei

Department of Chemical Engineering, Islamic Azad University, Mahshahr, Iran, emails: Mostafa.tabatabaee@yahoo.com (S.M.T. Ghomsheh), Alireza_azimi550@yahoo.com (A. Azimi), Mirzaei_fateme@yahoo.com (M. Mirzaei)

Received 14 August 2019; Accepted 6 June 2020

ABSTRACT

In this work, the novel highly-efficient thin film nanocomposite (TFN) FO membranes were fabricated. The support layer of FO membranes was prepared by blending hydrophilic polydopamine nanoparticles (PDA NPs) into polyphenylsulfone (PPSU) matrix using phase inversion method. The polycarbonate (PC) active layer of TFN membranes was prepared through interfacial polymerization on the surface of PPSU substrate and ultraviolet (UV) light surface treatment was considered for surface modification of PC active layer. The prepared TFN FO membranes were characterized by scanning electron microscopy, atomic force microscopy, Fourier-transform infrared spectroscopy, and hydrophilicity analysis. The modified TFN FO membranes by the incorporation of 1 wt.% PDA NPs into the substrate and UV surface treatment for 6 h exhibited the most promising results by showing high FO flux ($59.6 \text{ L m}^{-2} \text{ h}^{-1}$) and low reverse solute flux ($3.1 \text{ g m}^{-2} \text{ h}^{-1}$). To the best of our knowledge, this is the first study to report the effect of polydopamine nanoparticles and UV surface treatment on FO performance, and the results demonstrate the potential use of these modifications in TFN FO membrane fabrication.

Keywords: Polydopamine; Membrane; Forward osmosis; Thin film nanocomposite; UV treatment

1. Introduction

In the last decade, forward osmosis (FO) has been emerging as a potential cost-effective process in water treatment [1,2]. This evolving process is preferred in separation due to no need for hydraulic pressure and high disposal of different types of contaminants, resulting in less irreversible fouling on the FO membrane surface compared to pressure-driven membranes such as reverse osmosis [3]. However, all drawbacks of FO process such as high concentration polarization (CP), lower flux, and reverse solute diffusion (RSD) limit the performance of the FO applications [4,5]. So focus on the development of new membrane materials to solve these drawbacks is inevitable. Recently, thin-film composite (TFC) membranes prepared by interfacial polymerization

(IP) or dip coating followed by crosslinking are the most widely used in the FO applications [6–8]. Generally, an ideal TFC FO membrane should have a thin active layer with high water permeability and low salt permeability, and a porous support layer with high hydrophilicity, stability, mechanical strength, and smaller structural parameter in order to minimize the fouling propensity [9,10]. To achieve this purpose, some of the researches related to FO membranes have focused on support and active layer modification [11–13]. Recently, incorporation of nanofillers into the substrate and active layer of thin-film nanocomposite (TFN) FO membrane is an emerging technique to attain improved performance in FO. According to the literature, researchers have begun to use graphene oxide (GO) [14],

* Corresponding author.

carbon nanotubes (CNTs) [15], zeolites [16], clay [17], mesoporous silica [18], metal organic frameworks (MOFs) [19], etc., into FO membrane modification. These additives with hydrophilic nature and porous structure could effectively influence on substrate and active layer properties such as hydrophilicity and porosity. Also, the creation of water channels in the dense active layer is another result of the addition of nanomaterials that results in an increase in the water permeate of membranes [20]. Moreover, UV light as a tool for surface modification of polymeric materials has been explored in recent years [21,22]. Many researchers describes that the improving of surface hydrophilicity is due to the emergence of new hydrophilic oxygen-containing groups on the surface, such as hydroxyl, carboxyl, etc. [23]. During UV-irradiation process, at first the excited molecules can be formed, then the secondary step such as chain scission, cross-linking, and oxidation take place [24]. In the present study, thin film nanocomposite forward osmosis (TFN FO) membranes were fabricated based on the polyphenylsulfone (PPSU) substrate and polycarbonate (PC) active layer. Hydrophilic polydopamine nanoparticles (PDA NPs) were used as additives into substrate to improve forward osmosis (FO) membrane properties. Furthermore, the surface of PC active layer treated by UV light with the aim of improving its surface properties. The effect of the PDA NPs addition and UV light surface treatment on the membrane morphology, chemical composition, and roughness of the novel TFN-FO membranes were systematically investigated using various characterization methods.

2. Experimental

2.1. Materials

Dopamine hydrochloride (DA-HCl, Yuanye Biotechnology Co., Ltd., Shanghai, China), ethanol (99%, Sigma-Aldrich, Germany), and pure ammonia (99.8%, Linq Hengchang Chemical Co., Ltd., China) used to prepare PDA nanoparticles. Polyphenylsulfone (PPSU) ($M_w = 48,000$) was purchased from Solvay (Belgium). N-methyl-2-pyrrolidone (NMP, 99.5%) was supplied from Merck (Germany). Analytical grade and high purity dichloromethane were supplied from SAMCHUN (Korea). Bisphenol-A (BPA) was purchased from Loba Chemie Laboratory (Mumbai, India). *p*-cumylphenol, sodium hydroxide, and pyridine supplied from QRec. Phosgene solution (15 wt.% in toluene) was purchased from Sigma-Aldrich (Germany).

2.2. Polydopamine nanoparticle synthesis

Polydopamine nanoparticles (PDA NPs) were prepared by the oxidation of dopamine spontaneously under alkaline conditions at room temperature ($\sim 25^\circ\text{C}$) following the procedures described by Batul et al. [25]. Briefly, DA (10 mg mL^{-1}), was dissolved in the mixed solution of DI water, ethanol, and ammonia first under stirring in the presence of air oxygen until the colorless solution visually turned to pale yellow and then brownish black. After that, prepared particles were sedimented by centrifugation at 20,000 rpm for 15 min, followed by thoroughly rinsing with DI water and drying in oven at 80°C for 4 h.

2.3. Preparation of the mixed matrix substrate

The mixed matrix substrates were synthesized by using a phase separation technique. At first, PDA NPs (0.5, 1, 1.5, and 2 wt.%) were dispersed in the NMP followed by a 48 h ultra-sonication to minimize agglomeration. The polyphenylsulfone (PPSU) (16 wt.%) was added to the each of PDA NPs solution and the mixture was further sonicated for 2 d until a homogeneous solution was formed. After that, the resulting homogeneous dope solution was stored at room temperature for more than 24 h for degassing. This homogenous suspension was casted with 250 μm casting knife onto a glass plate, followed by immersion into a water bath at ambient temperature immediately to induce phase inversion.

2.4. Thin film nanocomposite fabrication

TFN polycarbonate membranes were prepared on the top side of PPSU/PDA NPs nanocomposite substrate by interfacial polymerization. In this way, phosgene (10.85 g, 36.6 mmol) was poured on to the top surface of substrate. Subsequently, an aqueous sodium hydroxide solution (5.25 g, 131.4 mmol), pyridine (0.12 mL) and bisphenol-A (BPA) (5 g, 21.9 mmol) in dichloromethane were added to the phosgene. Afterwards, *p*-cumylphenol (6.57 g, 21.9 mmol) was added to control the molecular weight of the polymer and stirred for 6 h at room temperature. After the formation of the polycarbonate layer, the organic phase was washed with an aqueous hydrochloride solution (37% w/w in water) and water. Finally, the remained solvent was removed by devolatilization and the membrane was kept in distilled water until that it was tested [26].

2.5. Hydrophilicity modification of polycarbonate active layer by ultraviolet (UV) light surface treatment

UV light surface treatment was used to enhance active layer hydrophilicity. For this purpose, membranes were cut into $6\text{ cm} \times 6\text{ cm}$ pieces and were cleaned using an ultrasonic bath of water and isopropyl alcohol (70% (v/v)) for 15 min at an ambient temperature. After drying, the samples were placed into the UV cabinet below the UV lamp. The modification of membranes surface were done by using UV radiation of two different wavelengths (254 and 365 nm). UV at a constant intensity of 359 and $265\ \mu\text{W cm}^{-2}$ were irradiated on the surfaces for 2, 4, and 6 h. Then the UV-treated membranes were subjected to characterization methods. A schematic diagram of the preparation process of the modified nanocomposite forward osmosis membrane is given in Fig. 1.

2.6. Characterization of polydopamine nanoparticles (PDA NPs)

The particle size distribution of the PDA NPs was measured by photon correlation spectroscopy (PCS) (photon correlator Brookhaven BI 9000 AT) that equipped with a laser source (coherent: 532 nm, 400 mW). The suspension was prepared by dispersing the PDA NPs in distilled water (concentration was around 0.1 g L^{-1}) and treated for 6 min in an ultrasonic bath to obtain a well-dispersed suspension.

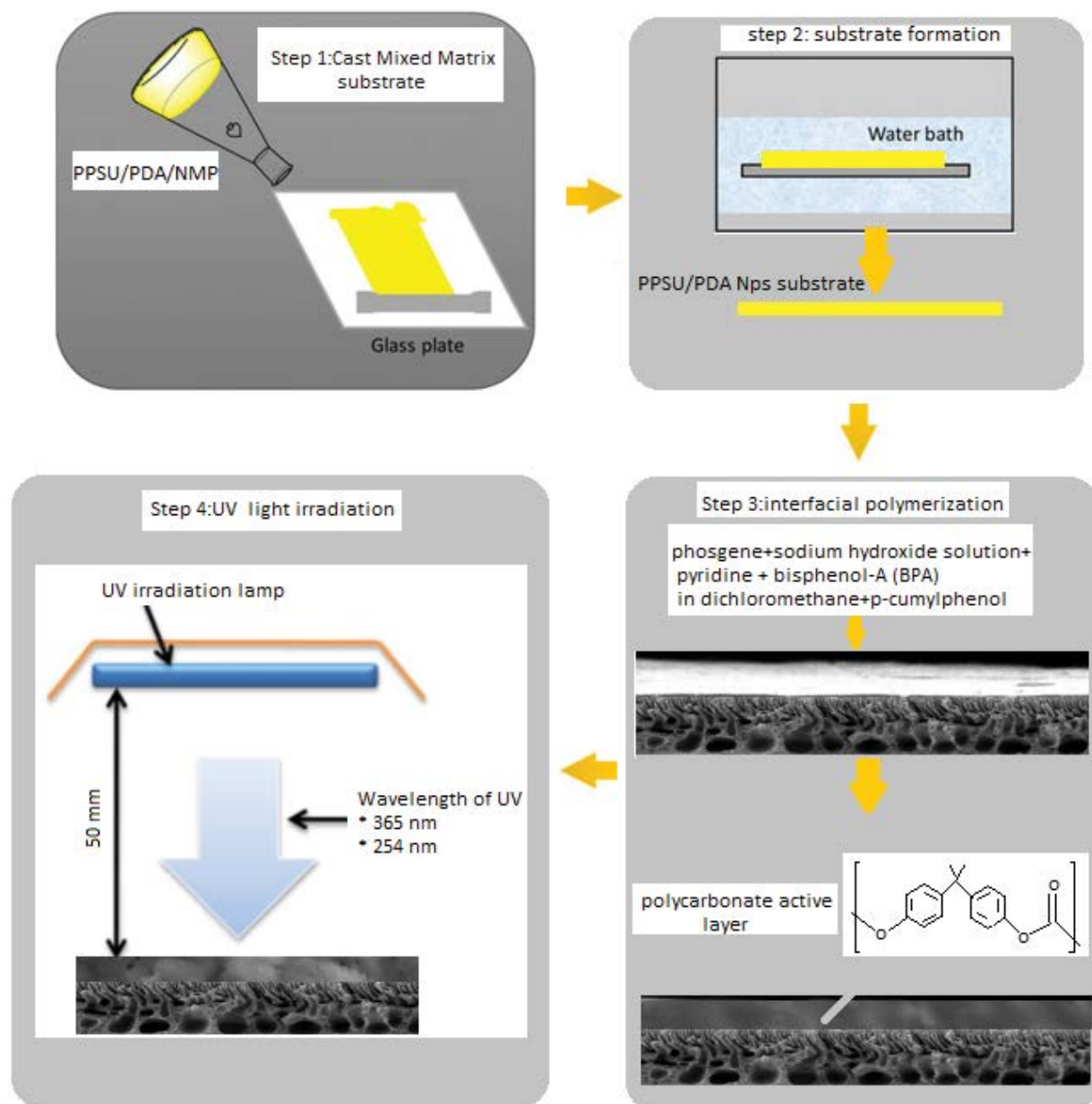


Fig. 1. Schematic diagram of the preparation process of the modified nanocomposite forward osmosis membrane.

Fourier transform infrared spectroscopy (FTIR) of DA powder and PDA NPs were measured by a Nicolet iS20 Fourier-transform infrared spectroscope (Waltham, MA, USA) to determine characteristic functional groups before and after polymerization of DA.

The structure of PDA NPs was observed by using a JSM-IT500HR (JEOL, USA) working at 200 kV.

2.7. Membrane characterization

The surface and cross-sectional morphologies of membranes were observed by SEM (JSM-IT500HR, USA). The functional groups of prepared membranes were identified by a Nicolet iS20 Fourier-transform infrared (FTIR) spectroscope (Waltham, MA, USA).

Membrane surface hydrophilicity was determined by contact angle using an optical contact angle measuring system (OCA 25-PMC 750, Germany) that is equipped with standard software to analyze the drop image for the calculation of surface free energy (SFE).

The SFE of the PC was determined by Owens-Wendt method [27] as represented by follow equation:

$$\left(\gamma_s^d \gamma_l^d\right)^{0.5} + \left(\gamma_s^p \gamma_l^p\right)^{0.5} = 0.5 \gamma_l (1 + \cos \theta) \quad (1)$$

where γ_l , γ_l^d , and γ_l^p are the SFE of a measuring liquid, dispersion, and polar components of the liquid SFE respectively. γ_s^d and γ_s^p are the dispersion and polar components of the solid.

Atomic force microscopy (AFM) was carried out to analyze the surface roughness of the membranes using AFM (Veeco, D9000 model, USA) by scanning the membrane surface over $10 \mu\text{m} \times 10 \mu\text{m}$ dimensions.

The membrane porosity (ϵ) was defined as the volume of the pores divided by the total volume of the membrane and was recorded using Eq. (2) [28]:

$$\epsilon = \frac{(m_1 - m_2) / \rho_w}{\frac{m_1 - m_2}{\rho_w} + m_2 / \rho_p} \quad (2)$$

where m_1 (g) and m_2 (g) are wet and dry weights, ρ_w is density of water, and ρ_p is density of polymer.

2.8. Evaluation of TFN membranes separation properties

Pure water permeability (A) and salt permeability coefficient (B) were measured by using a lab-scale cross flow filtration unit under the RO mode. The water permeability was determined from the pure water permeation flux under a trans-membrane pressure of 3.0 bar as describing following equations [11]:

$$J = \frac{\Delta V}{S_m \Delta t} \quad (3)$$

$$A = \frac{J}{\Delta P} \quad (4)$$

where S_m is effective membrane area, ΔV is permeate volume collected at measuring time interval Δt and ΔP is trans-membrane pressure difference.

The salt permeability, B , was evaluated by [29,30]:

$$B = A \frac{(1 - R)(\Delta P - \Delta \pi)}{R} \quad (5)$$

$$R = 1 - \frac{C_p}{C_f} \quad (6)$$

where $\Delta \pi$ is the osmotic pressure difference across the membrane. Also, The C_f and C_p are measured feed and permeate concentrations respectively which were measured in terms of conductivity by conductivity meter (Lutron Digital Conductivity Meter CD-4303HA METER) using 20 mM NaCl solution as a feed.

2.9. Evaluation of TFN FO membranes performance

The FO experiments were conducted through a laboratory scale cross flow fabricated FO setup with an effective filtration area of 20.2 cm². All tests were conducted at ambient temperature. In these tests, NaCl solution (15 mM) was used as feed solution and 1 M NaCl as draw solution.

The operation mode is active layer facing feed solution. Both solutions were circulated at a volumetric flow rate of 0.25 L min⁻¹ and were recirculated during experiments. Each

experiment lasted for 1 h and was repeated three times to obtain more accurate results. The weight changes of draw solution were recorded by an electronic balance to calculate water flux (J_v) while the feed solution conductivity was recorded to calculate reverse salt flux (J_s). J_v and J_s were calculated by Eqs. (7) and (8) [18]:

$$J_v = \frac{\Delta V}{S_m \Delta t} \quad (7)$$

$$J_s = \frac{\Delta C V}{S_m \Delta t} \quad (8)$$

where ΔV is the volume of water permeating through the membrane (L) over a given period of time (Δt) (h), S_m is the effective area of the FO membrane (m²), C (g L⁻¹) is the feed solution concentration, and V (L) is the volume of feed solution over Δt , respectively.

3. Results and discussion

3.1. Characterization of polydopamine nanoparticles (PDA NPs)

The morphology of PDA NPs was characterized by scanning electron microscopy (SEM) as shown in Fig. 2. As indicated in the SEM image, PDA NPs obtained are near monodisperse with uniform spherical morphology. FTIR spectroscopy of DA powder and PDA NPs were measured to determine characteristic functional groups before and after polymerization of DA (Fig. 3). The FTIR spectrum of DA showed characteristic peaks at 3,110 cm⁻¹, which is attributed to the O–H stretching vibrations. The characteristic bands at 1,462 and 1,475 cm⁻¹ assigned as the benzene ring stretching vibrations. Also, there are several characteristic bands of DA can be identified including C–O–H bending vibration at 1,320 cm⁻¹, C–O symmetry vibration at 1,173 cm⁻¹ and C–C stretching vibration at 1,166 cm⁻¹, respectively.

At FTIR spectrum of PDA NPs, the broad band from 3,200 to 3,500 cm⁻¹ is attributed to O–H stretching vibrations such as a catechol group. The characteristic peaks at 1,503 and 1,154 cm⁻¹ are attributed to the stretching of aromatic C=C bonds of indole and C–N bending in indoline respectively. From FTIR results, it can be concluded that the presence of indole and indoline structures in FTIR spectrum of PDA proved the successful polymerization of DA to PDA.

Fig. 4 shows particle size distribution was obtained by PCS. Mean and median sizes obtained with PCS are 210 and 195 nm, respectively. The zeta potential of the PDA particles was measured to be approximately –40 mV.

3.2. Membrane characterization

3.2.1. Contact angle and porosity measurements

The water contact angle on the polycarbonate surface of TFN membranes as a function of treatment in UV radiation of two wavelengths (254 and 365 nm) are illustrated in Fig. 5. As can be seen the water contact angle decreased from 82° for untreated UV membrane to 61° for UV treated membrane after 6 h of treatment in UV radiation of wavelength 254 nm.

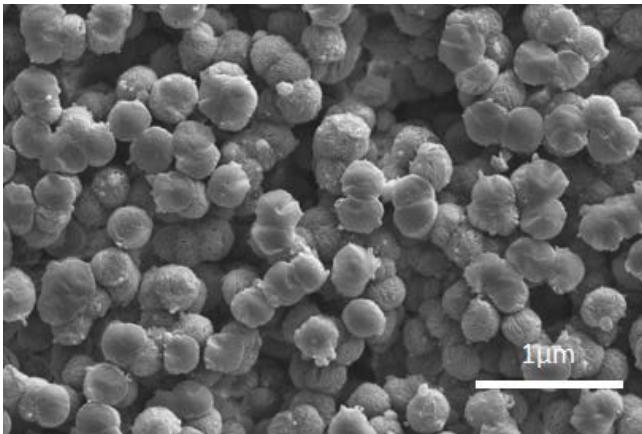


Fig. 2. SEM image of PDA nanoparticles.

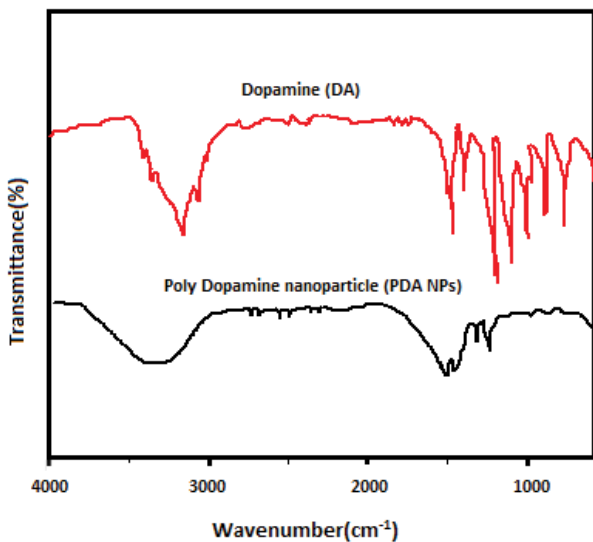


Fig. 3. FTIR spectra of dopamine and polydopamine nanoparticle.

Also, reduction in contact angle (nearly 5°) by the treatment in UV radiation of 365 nm was observed. The UV radiation of wavelength 254 nm related to photons of energy 4.8 eV whereas the radiation of wavelength 365 nm corresponds to photons of energy 3.4 eV. Generally, the higher level of photons energy of short-wavelength is the reason for more effective treatment compared to the longer wavelength.

Generally, ultraviolet (UV) treatment results in creating active sites on PC surface. These active sites emerge due to bond scission that resulted by the UV treatment. The active sites can interact to air oxygen and formed hydrophilic functional group such as hydroxyl. So, these functional groups were reason of hydrophilicity changes.

The total SFE of the sample calculated from two liquid model as described in section 2.7 (Membrane characterization). Fig. 6 reveals the total SFE of PC surface vs. time of UV treatment at two wavelengths (254 and 365 nm). As can be seen, the SFE of the PC increases with treatment time at shorter wavelength (254 nm) while UV treatment in longer wavelength (365 nm) has no significantly effect.

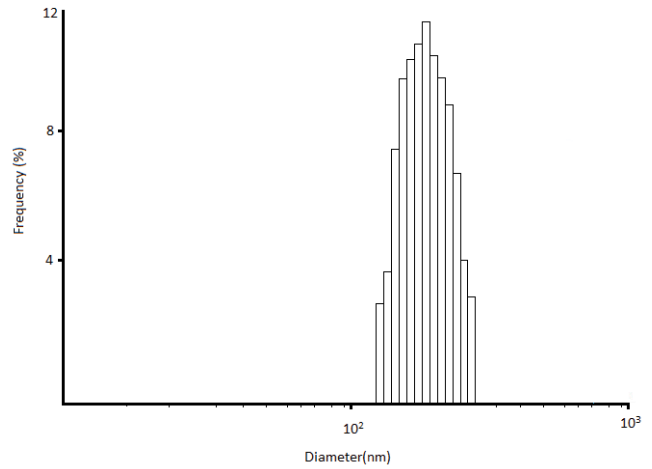


Fig. 4. Size distribution of PDA NPs measured by PCS.

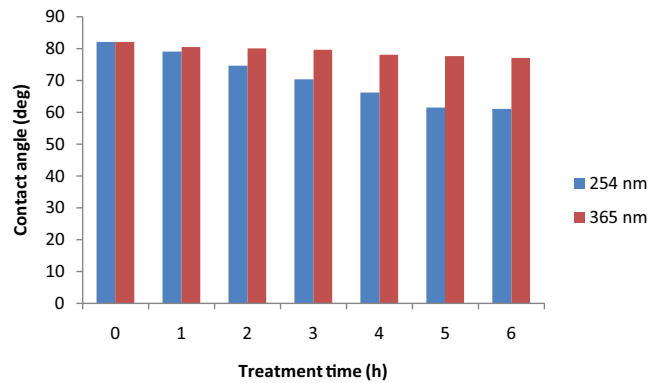


Fig. 5. Contact angle of PC surface of TFN FO membrane with treatment time at two different wavelengths (PDA NPs in substrate: 1 wt.%).

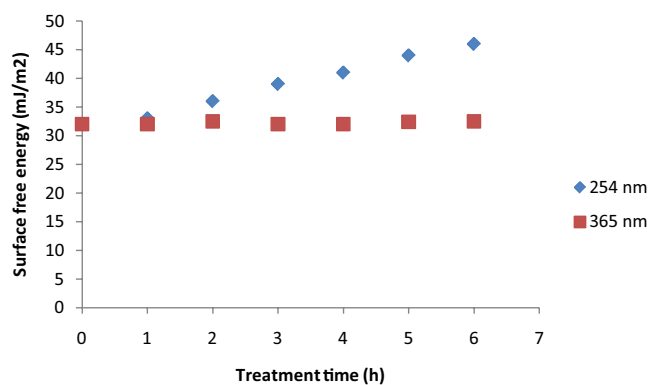


Fig. 6. Surface free energy of TFN FO membrane with treatment time at two different wavelengths (PDA NPs in substrate: 1 wt.%).

The porosity data of membranes are presented in Fig. 7. As can be seen, an increment in the membrane porosity was observed for all modified FO membranes by increasing PDA NPs up to 1 wt.% compared to the unmodified membrane. This might be explained by the fact that the

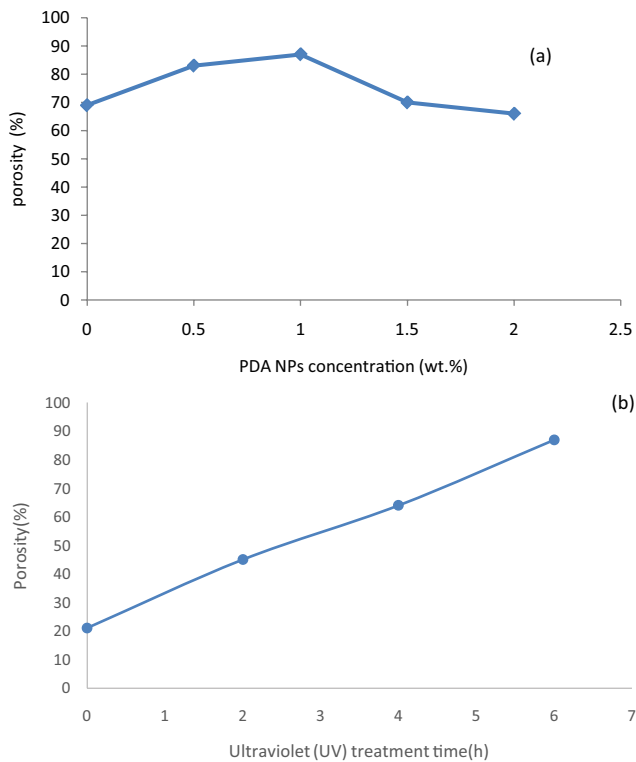


Fig. 7. Effect of (a) polydopamine nanoparticles concentration on porosity of FO membranes (ultraviolet (UV) treatment time: 6 h) and (b) ultraviolet (UV) treatment time on porosity of FO membranes (wavelength: 254 nm and PDA NPs in substrate: 1 wt.%).

hydrophilic PDA NPs can strongly influence on the rate of the solvent/non-solvent exchange during the phase inversion process. also, further increasing in PDA NPs concentration (>1 wt.%), resulted in the increased viscosities of the dope solutions resulted in reduced rate of the solvent/non-solvent exchange during the phase separation to formless porous structures [31,32]. Also these results showed that ultraviolet light surface treatment has an increasing effect on the surface porosity (Fig. 7b). These results are in agreement with that of SEM analysis.

3.2.2. FTIR analysis

FTIR spectroscopy was used for evaluating chemical structure of the TFN FO membranes (Fig. 8). The broad band from 3,000 to 3,600 cm^{-1} is attributed to the stretching modes of N–H and O–H bonds of PDA NPs. Moreover, the peak at 1,558 and 1,506 cm^{-1} is due to the stretching of aromatic C=C bonds of indole, and the peak at 1,166 cm^{-1} was corresponding to C–N bending in indoline of PDA NPs that embedded in the polyphenylsulfone.

In the TFN membrane with non-ultraviolet light surface treatment, the characteristic absorption bands of PC, observed in the region 1,600–1,800 cm^{-1} , attribute to the C=O stretching vibration of carbonate groups. By ultraviolet (UV) light surface treatment the relative decrease in the intensity of the C=O stretching vibration was observed ($\approx 1,650$ cm^{-1}). It's due to the chain breaking at the carbonate site where

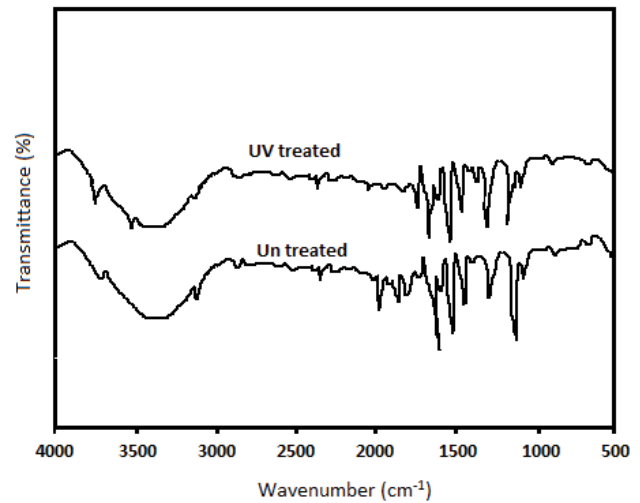


Fig. 8. FTIR spectra of untreated and UV treated TFN FO membrane (PDA NPs in substrate: 1 wt.%).

hydroxyl groups are formed. Moreover, there are several characteristic bands of PPSU substrate can be identified including C=C stretching vibration at 1,479 and 1,583 cm^{-1} , and asymmetric/symmetric stretching of O=S=O at 1,293 and 1,169 cm^{-1} .

3.2.3. AFM analysis

Surface AFM images of TFN FO membranes are shown in Fig. 9. These images confirm that the non-UV treated membrane has smoother structure than the UV treated TFN FO membrane. This might explained by the fact that UV irradiation treatment of PC surface of TFN FO membranes resulting in a surface energy increases, so surface chemistry may be modified. From this Fig. 9, it's obvious that the protuberances and wave type micropatterns appeared on the UV treated PC surfaces in which the root-mean-square (RMS) roughness of surface increased from 1.6 nm (for non-UV treated PC surface) to 2.5 nm (for UV treated PC surface) as the treatment time increases up to 6 h.

3.2.4. SEM analysis

Fig. 10 is shown the SEM images of the cross section of the PPSU/PDA NPs substrate and surface structure of TFN FO membranes. As can be seen from the cross-section structure substrate of nanocomposite membrane, all the membranes demonstrate an asymmetric structure with a dense top layer supported on a bottom finger-like structure layer. It's clear that there is no significant difference between the modified and unmodified membrane's substrate structure. But PDA NPs significantly affected on the porosity of the PPSU substrate. The presence of affinity and interaction between PDA NPs and water as the coagulant provides a great permeation velocity of water into nascent membrane during the phase inversion, so leads to the more regular formation of macrovoids and transverse cavities in PDA NPs embedded PPSU substrate.

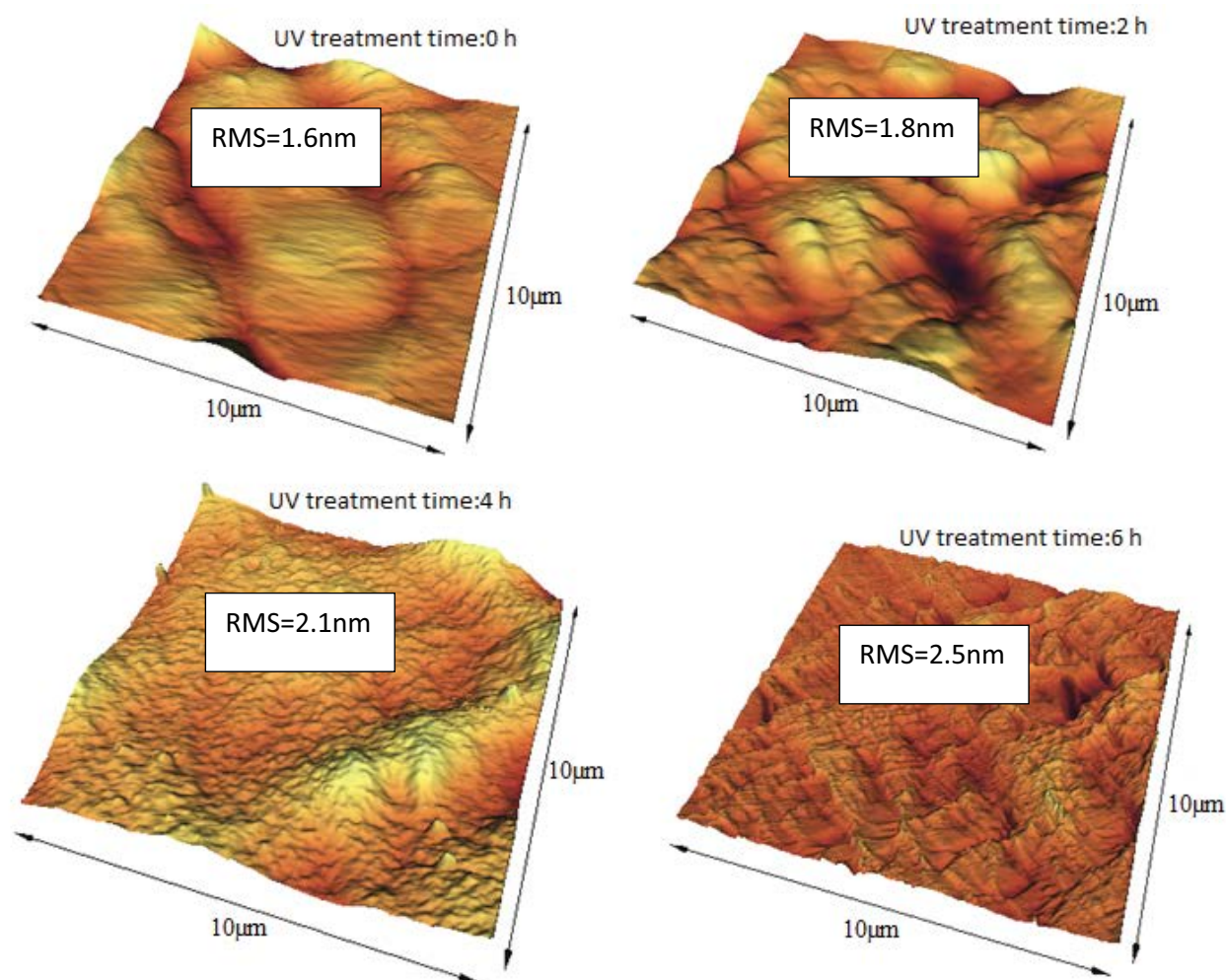


Fig. 9. AFM images of TFN FO membrane at different UV treatment time (PDA NPs in substrate: 1 wt.%).

By increasing PDA NPs concentration (≥ 1 wt.%), as a result of increased viscosity, the liquid–liquid demixing process is delayed and the phase separation process is finally dominated by the solid–liquid demixing. Therefore membrane with less porosity was formed.

Surface views of the TFN FO membrane demonstrate that untreated PC surface has a smooth structure. By treating PC surface with UV irradiation for 6 h, prominent surface changes were appeared on the surface of membranes.

3.2.5. Separation properties of TFN membranes

Table 1 represents the water permeability and solute permeability of TFN membranes during RO test. As can be seen, all of the modified TFN FO membranes show a better water permeability comparing to the unmodified TFN FO membrane. In fact incorporation of PDA NPs in the PPSU substrate and UV irradiation treatment of PC active layer significantly improved hydrophilicity of PPSU substrate and PC active layer as well as the enlargement of pore size and porosity of them, so the enhancement of TFN membrane performance was achieved. Generally, salt rejection of the TFN membranes is mainly dependent

on the selective active layer [33]. By UV treatment of PC surface during 6 h an increase in solute permeability is observed. This is most probably due to the surface changes created on the membrane such as increased porosity.

Also the ratio of solute permeability to water permeability (B/A) is presented in Table 1. As known the B/A ratio is an important parameter for reverse salt flux evaluation so that smallest value of this ratio leads to less reverse salt diffusion from the draw solution into the feed solution in the FO process [12].

By considering the high water permeability, low solute permeability, and low B/A ratio, the (PPSU/(1 wt.% PDA NPs))/PC TFN FO membrane treated by UV for 4 h exhibits good potential for FO application.

3.2.6. FO performance of TFN membranes

The performance of TFN FO membranes were evaluated in terms of water flux and reverse salt flux. Figs. 11a and b illustrate a comparison of the average water flux of unmodified and modified membranes during the FO operation using 15 mM NaCl as the feed solution and 1 M NaCl as the draw solution. As can be seen, the water flux is related

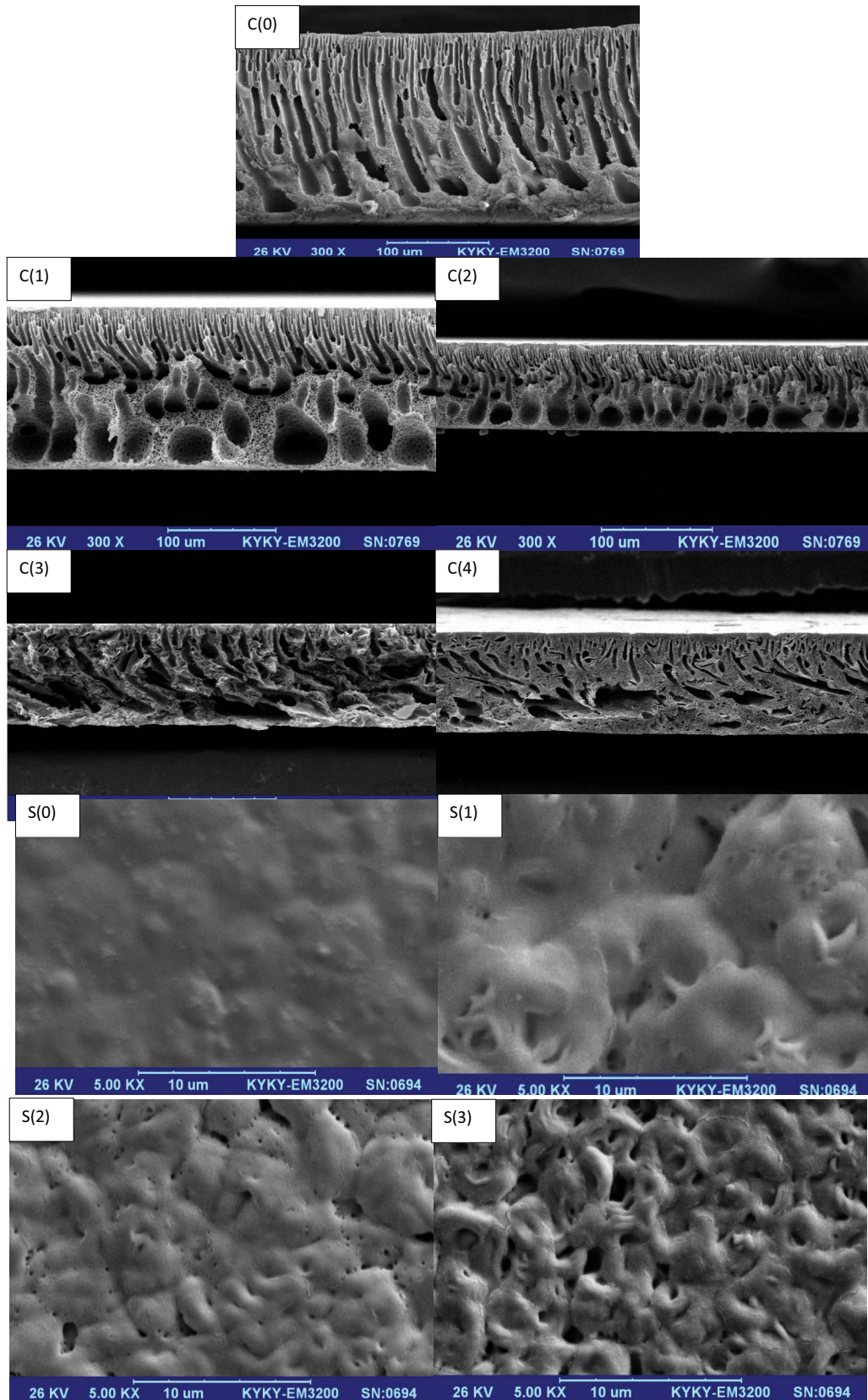


Fig. 10. SEM images of prepared TFN FO membranes, C(0): 0 wt.% PDA NPs, C(1): 0.5 wt.% PDA NPs, C(2): 1 wt.% PDA NPs, C(3): 1.5 wt.% PDA NPs, C(4): 2 wt.% PDA NPs, S(0): UV treatment time:0 h, 0 wt.% PDA NPs, S(1): UV treatment time:2 h, 0 wt.% PDA NPs, S(2): UV treatment time:4 h, 0 wt.% PDA NPs, S(3): UV treatment time:6 h, 0 wt.% PDA NPs, C: cross and S: surface.

Table 1
Separation properties of TFN FO membranes

Membrane	Water permeability (A) (L m ⁻² h ⁻¹ bar)	Solute permeability (B) (g m ⁻² h ⁻¹)	(B/A) bar
(PPSU/1 wt.% PDA NPs)/PC UV treatment time:0 h	2.7	0.4	0.14
(PPSU/1 wt.% PDA NPs)/PC UV treatment time:2 h	3.4	0.43	0.12
(PPSU/1 wt.% PDA NPs)/PC UV treatment time:4 h	5.6	0.45	0.08
(PPSU/1 wt.% PDA NPs)/PC UV treatment time:6 h	6.1	0.49	0.08

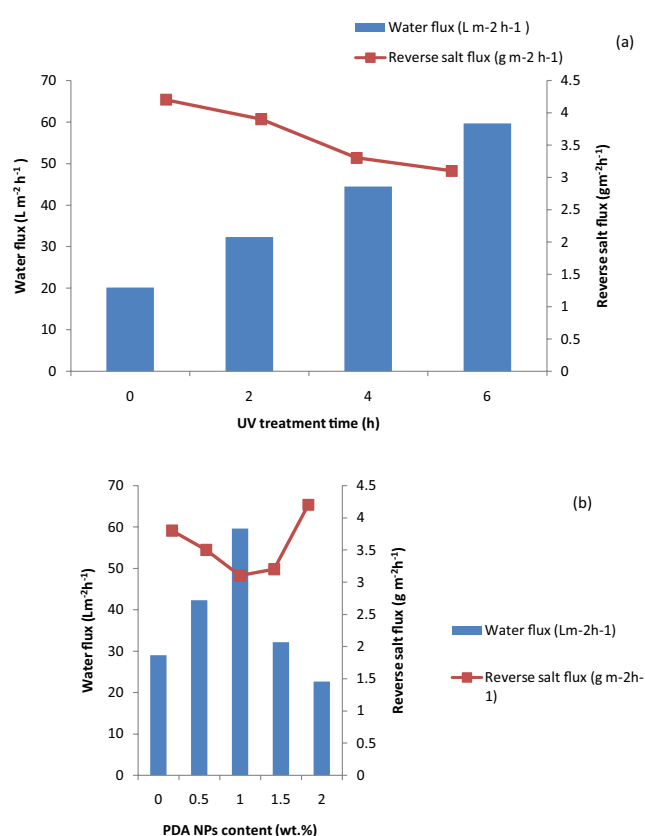


Fig. 11. Water flux and reverse salt flux of (a) (PPSU/1 wt.% PDA NPs)/PC at various UV treatment time and (b) modified PPSU substrate by different concentration of PDA NPs for 6 h treatment time.

to PPSU substrate property (porosity and hydrophilicity) changes upon the addition of PDA NPs. The incorporation of PDA NPs up to 1 wt.% favored the formation of more macrovoid structures, contributing to the porosity and reduced ICP during FO permeation. In addition, water flux was found to be influenced by the hydrophilic functional group that created on the PC surface as a result of UV treatment. When PC surface treated by UV irradiation, further enhancement in water flux of membranes was observed.

Generally by UV irradiation, PDA NPs modified TFN FO membranes exhibits higher water flux than unmodified TFN FO membrane with slight decrease in solute reverse flux. The (PPSU/1 wt.% PDA NPs)/PC membrane by UV treatment time of 6 h showed a water flux of about 59.6 L m⁻² h⁻¹ with salt reverse flux of 3.1 g m⁻² h⁻¹ whilst these values for unmodified surface membrane 20.2 L m⁻² h⁻¹ and 4.2 g m⁻² h⁻¹ were respectively obtained. On the other hand, the higher roughness of modified membranes can be improved the surface hydrophilicity. It was attributed to increased PC surface area which increases the transition rate of water molecules, thus leading to such water flux enhancement [34]. The descending trend for reverse salt flux by UV treatment time is due to the effect of roughness of the surface which occurs with increasing treatment time.

The effect of draw solute concentration on the FO performance of TFN membranes is evaluated and the results are presented in Fig. 12. As shown, reverse salt flux slightly increases with the increase in the draw solution concentration, which is attributed to their high osmotic pressure. also, by increasing draw solute concentration the water flux for all of modified TFN membranes has an ascending trend due to the high driving force caused by high salt concentration. It should be noted that the water flux increment at high salt concentration show a nonlinear behavior which is most probably due to dilutive ICP within the substrate [35].

4. Conclusion

Modification of new TFN FO membranes were carried out by the addition of different values of polydopamine nanoparticles into the PPSU substrate and UV surface treatment of poly carbonate active layer. The effect of PDA NPs concentration and UV treatment time were evaluated on the membrane specifications including morphology, roughness, chemical structure, contact angle, and FO performance. Results showed that TFN FO membranes hydrophilicity were changed by the addition of polydopamine nanoparticles into the substrate and UV surface treatment of poly carbonate active layer, with porosity increasing (up to 1 wt.%). The water contact angle decreased from 82° for untreated UV (PPSU/1 wt.% PDA NPs)/PC membrane to 61° for UV (PPSU/1 wt.% PDA NPs)/PC treated membrane after 6 h of treatment in UV radiation of wavelength 254 nm.

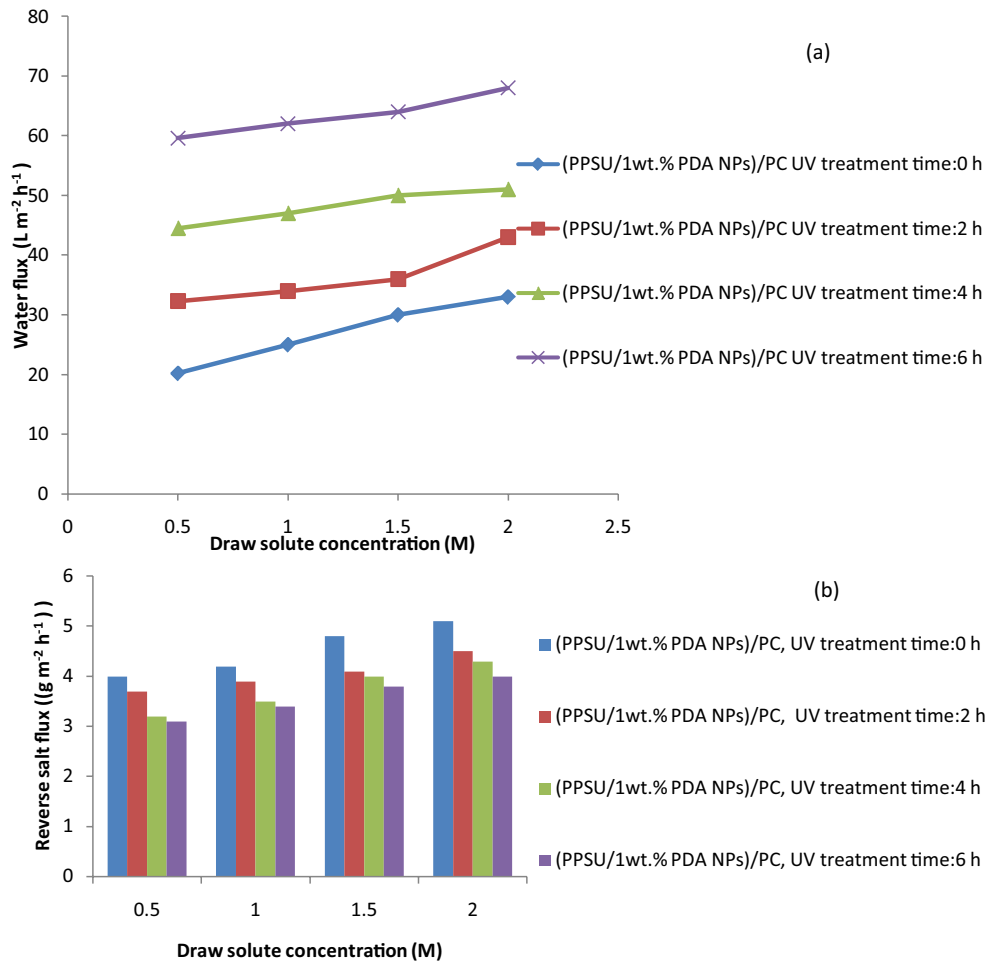


Fig. 12. Effect of draw solute concentration on (a) water flux and (b) reverse salt flux of (PPSU/1 wt.% PDA NPs)/PC at various UV treatment time.

Ultraviolet (UV) treatment results in creating active sites on PC surface which can interact to air oxygen and formed hydrophilic functional group. These functional groups were responsible for hydrophilicity improvement. Furthermore, the UV surface treatment up to 6 h increased the surface roughness of the membranes. FO performance through the prepared membranes was noticeably affected by the PDA NPs addition and UV surface treatment time according to their direct effect on the membrane structure and surface porosity. The FO water flux of about $59.6 \text{ L m}^{-2} \text{ h}^{-1}$ and reverse solute flux of about $3.1 \text{ g m}^{-2} \text{ h}^{-1}$ were achieved by modification of membranes with polydopamine and ultraviolet (UV) surface treatment. Finally, this study demonstrated that the FO membrane modification with polydopamine nanoparticles and UV surface treatment of its active layer have great potential for FO application as a result of their improved structural and separation properties.

References

- [1] W. Xu, Q. Chen, Q. Ge, Recent advances in forward osmosis (FO) membrane: chemical modifications on membranes for FO processes, *Desalination*, 419 (2017) 101–116.
- [2] D. Emadzadeh, W.J. Lau, T. Matsuura, M. Rahbari-Sisakht, A.F. Ismail, A novel thin film composite forward osmosis membrane prepared from PSf-TiO₂ nanocomposite substrate for water desalination, *Chem. Eng. J.*, 237 (2014) 70–80.
- [3] N. Ghaemi, Z. Khodakarami, Nano-biopolymer effect on forward osmosis performance of cellulosic membrane: high water flux and low reverse salt, *Carbohydr. Polym.*, 204 (2018) 78–88.
- [4] K. Lutzmiah, A.R.D. Verliefde, K. Roest, L.C. Rietveld, E.R. Cornelissen, Forward osmosis for application in wastewater treatment: a review, *Water Res.*, 58 (2014) 179–197.
- [5] S. Zhao, L. Zou, C.Y. Tang, D. Mulcahy, Recent developments in forward osmosis: opportunities and challenges, *J. Membr. Sci.*, 396 (2012) 1–21.
- [6] M. Tian, Y.N. Wang, R. Wang, A.G. Fane, Synthesis and characterization of thin film nanocomposite forward osmosis membranes supported by silica nanoparticle incorporated nanofibrous substrate, *Desalination*, 401 (2017) 142–150.
- [7] T. Ni, Q. Ge, Highly hydrophilic thin-film composition forward osmosis (FO) membranes functionalized with aniline sulfonate/bisulfonate for desalination, *J. Membr. Sci.*, 564 (2018) 732–741.
- [8] L. Shen, J. Zuo, Y. Wang, Tris(2-aminoethyl)amine *in-situ* modified thin-film composite membranes for forward osmosis applications, *J. Membr. Sci.*, 537 (2017) 186–201.
- [9] H.Y. Ng, W. Tang, W.S. Wong, Performance of forward (direct) osmosis process: membrane structure and transport phenomenon, *Environ. Sci. Technol.*, 40 (2006) 2408–2413.

- [10] J. Wei, C. Qiu, C.Y. Tang, R. Wang, A.G. Fane, Synthesis and characterization of flat-sheet thin film composite forward osmosis membranes, *J. Membr. Sci.*, 372 (2011) 292–302.
- [11] Z. Dabaghian, A. Rahimpour, M. Jahanshahi, Highly porous cellulosic nanocomposite membranes with enhanced performance for forward osmosis desalination, *Desalination*, 381 (2016) 117–125.
- [12] N. Niksefat, M. Jahanshahi, A. Rahimpour, The effect of SiO₂ nanoparticles on morphology and performance of thin film composite membranes for forward osmosis application, *Desalination*, 343 (2014) 140–146.
- [13] Y. Wang, R. Ou, Q. Ge, H. Wang, T. Xu, Preparation of polyethersulfone/carbon nanotube substrate for high-performance forward osmosis membrane, *Desalination*, 330 (2013) 70–78.
- [14] D. Qin, Z. Liu, D.D. Sun, X. Song, H. Bai, A new nanocomposite forward osmosis membrane custom-designed for treating shale gas wastewater, *Sci. Rep.*, 5 (2015) 1–14.
- [15] L. Dumée, J. Lee, K. Sears, B. Tardy, M. Duke, S. Gray, Fabrication of thin film composite poly(amide)-carbon-nanotube supported membranes for enhanced performance in osmotically driven desalination systems, *J. Membr. Sci.*, 427 (2013) 422–430.
- [16] N. Ma, J. Wei, R. Liao, C.Y. Tang, Zeolite-polyamide thin film nanocomposite membranes: towards enhanced performance for forward osmosis, *J. Membr. Sci.*, 405–406 (2012) 149–157.
- [17] B.K. Nandi, R. Uppaluri, M.K. Purkait, Effects of dip coating parameters on the morphology and transport properties of cellulose acetate-ceramic composite membranes, *J. Membr. Sci.*, 330 (2009) 246–258.
- [18] A. Shakeri, R. Razavi, H. Salehi, M. Fallahi, T. Eghbalazar, Thin film nanocomposite forward osmosis membrane embedded with amine-functionalized ordered mesoporous silica, *Appl. Surf. Sci.*, 481 (2019) 811–818.
- [19] Y. Xu, X.L. Gao, X.J. Wang, Q. Wang, Z.Y. Ji, X.Y. Wang, T. Wu, C.J. Gao, Highly and stably water permeable thin film nanocomposite membranes doped with MIL-101 (Cr) nanoparticles for reverse osmosis application, *Materials*, 9 (2016) 870–883, doi: 10.3390/ma9110870.
- [20] R. Kumar, M. Ahmed, B. Garudachari, J.P. Thomas, Evaluation of the forward osmosis performance of cellulose acetate nanocomposite membranes, *Arabian J. Sci. Eng.*, 43 (2018) 5871–5879.
- [21] T.N. Murakami, Y. Fukushima, Y. Hirano, Y. Tokuoka, M. Takahashi, Modification of PS films by combined treatment of ozone aeration and UV irradiation in aqueous ammonia solution for the introduction of amine and amide groups on their surface, *Appl. Surf. Sci.*, 249 (2005) 425–432.
- [22] M. Olbrich, G. Punshon, I. Frischauf, H.J. Salacinski, E. Rebollar, C. Romanin, A.M. Seifalian, J. Heitz, UV surface modification of a new nanocomposite polymer to improve cytocompatibility, *J. Biomater. Sci. Polym. Ed.*, 18 (2007) 453–468.
- [23] J. Lai, B. Sunderland, J. Xue, S. Yan, W. Zhao, M. Folkard, B.D. Michael, Y. Wang, Study on hydrophilicity of polymer surfaces improved by plasma treatment, *Appl. Surf. Sci.*, 252 (2006) 3375–3379.
- [24] C. Fischbach, J. Tessmar, A. Lucke, E. Schnell, G. Schmeer, T. Blunk, Does UV irradiation affect polymer properties relevant to tissue engineering?, *Surf. Sci.*, 491 (2001) 333–345.
- [25] R. Batul, A. Yu, M. Bhave, A. Khaliq, Synthesis of polydopamine nanoparticles for drug delivery applications, *Microsc. Microanal.*, 24 (2018) 1758–1759.
- [26] D.J. Brunelle, P.M. Smigelski, E.P. Boden, Evolution of polycarbonate process technologies, *ACS Symp. Ser.*, 89 (2005) 8–21.
- [27] D.K. Owens, R.C. Wendt, Estimation of the surface free energy of polymers, *J. Appl. Polym. Sci.*, 13 (1969) 1741–1747.
- [28] X. Song, L. Wang, C.Y. Tang, Z. Wang, C. Gao, Fabrication of carbon nanotubes incorporated double-skinned thin film nanocomposite membranes for enhanced separation performance and antifouling capability in forward osmosis, *Desalination*, 369 (2015) 1–9.
- [29] S.J. Shi, Y. Pan, S.F. Wang, Z. Dai, L. Gu, Q. Wu, Aluminosilicate nanotubes embedded polyamide thin film nanocomposite forward osmosis membranes with simultaneous enhancement of water permeability and selectivity, *Polymers*, 11 (2019) 879–895.
- [30] Y.H. Pan, Q.Y. Zhao, L. Gu, Q.Y. Wu, Thin film nanocomposite membranes based on imogolite nanotubes blended substrates for forward osmosis desalination, *Desalination*, 421 (2017) 160–168.
- [31] G.R. Guillen, Y. Pan, M. Li, E.M.V. Hoek, Preparation and characterization of membranes formed by nonsolvent induced phase separation: a review, *Ind. Eng. Chem. Res.*, 50 (2011) 3798–3817.
- [32] H. Susanto, M. Ulbrich, Characteristics, performance and stability of polyethersulfone ultrafiltration membranes prepared by phase separation method using different macromolecular additives, *J. Membr. Sci.*, 327 (2009) 125–135.
- [33] X. Li, K.Y. Wang, B. Helmer, T.S. Chung, Thin-film composite membranes and formation mechanism of thin-film layers on hydrophilic cellulose acetate propionate substrates for forward osmosis processes, *Ind. Eng. Chem. Res.*, 51 (2012) 10039–10050.
- [34] W. Ding, Y. Li, M. Bao, Ji. Zhang, C. Zhang, J. Lu, Highly permeable and stable forward osmosis (FO) membrane based on the incorporation of Al₂O₃ nanoparticles into both substrate and polyamide active layer, *RSC Adv.*, 7 (2017) 40311–40320.
- [35] G. Han, T.S. Chung, M. Toriida, S. Tamai, Thin-film composite forward osmosis membranes with novel hydrophilic supports for desalination, *J. Membr. Sci.*, 423 (2012) 543–555.